npj | genomic medicine

Article

Published in partnership with CEGMR, King Abdulaziz University

https://doi.org/10.1038/s41525-026-00566-z

Variants in the ciliopathy gene *SCLT1* are associated with non-syndromic and syndromic retinal degeneration of variable severity

Riccardo Sangermano[1], Kaoru Fujinami[2], Suk Ho Byeon[3], Emily M. Place[1], Julien Navarro[4], Johanna Valensi[5], Samer Khateb[5], Eyal Banin[5], Christel Condroyer[4], Stephanie DiTroia[6], Dror Sharon[5], Christina Zeitz[4], Isabelle Audo[4,7], Kinga M. Bujakowska[1] ✉ & Jinu Han[3] ✉

Inherited retinal degenerations (IRDs) are a group of clinically and genetically heterogeneous blinding disorders. In this study, we describe five families clearly or which were presumed to be diagnosed with autosomal recessive non-syndromic IRD and one with mild syndromic IRD, in which affected probands carried rare bi-allelic variants in *SCLT1*, a gene previously associated with multiple autosomal recessive ciliopathies. Eight of the ten variants identified were novel; five variants affected splicing, including the known missense p.(Lys544Arg), detected in compound heterozygosity in three East Asian probands, and the novel, hypomorphic, deep-intronic variant c.290+2732A>G, leading to the inclusion of a 45-bp cryptic exon containing a premature termination codon. Analysis of the genomic data also revealed a large in-frame tandem duplication spanning exons 3-10, which was subsequently validated. Although no clear correlation was found between the severity of the *SCLT1*-associated phenotypes and the identified causal variants, this report expands the current knowledge of *SCLT1*-associated disease by enriching its mutational landscape and clearly supports its association with autosomal recessive non-syndromic IRD.

Inherited retinal degenerations (IRDs) are a group of genetically and clinically heterogeneous Mendelian disorders characterized by a progressive loss of retinal rod and cone photoreceptors, specialized neuronal cells initiating vision. The incidence of IRDs has been estimated to be around 1 in 2000 individuals, with more than two million people affected worldwide[1]. IRDs can manifest as an isolated phenotype where only the retina is affected (i.e., non-syndromic IRDs), such as in rod-cone dystrophy (RCD), or as a syndromic disease, where retinal degeneration is one of many signs of a multiorgan clinical manifestation[2]. Syndromic IRDs often arise from defects in the primary cilium, a microtubule-based sensory organelle that projects from the plasma membrane of nearly every human cell, including the photoreceptors[3]. Absence or functional alteration of any of the primary cilium components leads to a spectrum of potential co-morbidities, referred to as ciliopathies, affecting millions of people worldwide[4].

The Sodium Channel and Clathrin Linker 1 *(SCLT1)* gene (OMIM# 611399), initially known as clathrin-associated protein-1A (*CAP-1A*) is a ciliary gene encoding a multidomain protein. SCLT1 was first discovered as a specific interactor of the voltage-gated sodium channel $Na_v1.8$ in nociceptive neurons, where it acts as a linker between clathrin and the sodium channel in multiprotein complexes, suggesting a role as an endocytic adaptor protein regulating $Na_v1.8$ density at the cell surface[5]. SCLT1 was later shown to be involved in ciliogenesis, as one of the core distal appendage

[1]Ocular Genomics Institute, Massachusetts Eye and Ear, Department of Ophthalmology, Harvard Medical School, Boston, MA, USA. [2]Laboratory of Visual Physiology, Division of Vision Research, National Institute of Sensory Organs, NHO Tokyo Medical Center, Tokyo, Japan. [3]Institute of Vision Research, Department of Ophthalmology, Severance Hospital, Yonsei University College of Medicine, Seoul, Republic of Korea. [4]Sorbonne Université, INSERM, CNRS, Institut de la Vision, Paris, France. [5]Department of Ophthalmology, Hadassah Medical Center, Faculty of Medicine, The Hebrew University of Jerusalem, Jerusalem, Israel. [6]Center for Mendelian Genomics, Broad Institute of Massachusetts Institute of Technology and Harvard, Cambridge, MA, USA. [7]Centre Hospitalier National d'Ophtalmologie des Quinze-Vingts, Centre de Référence Maladies Rares REFERET and INSERM-DGOS, Paris, France.
✉e-mail: kinga_bujakowska@meei.harvard.edu; jinuhan@yuhs.ac

(DAP) components of centrioles, a group of five proteins (CEP83, CEP89, SCLT1, CEP164, and FBF1) needed to anchor the primary cilium to the plasma membrane and promote cilia initiation[6]. In particular, SCLT1 is a key DAP member, as it is required for the recruitment of CEP164 and FBF1 at the mature centriole, also known as basal body[6].

Bi-allelic pathogenic variants in the *SCLT1* gene were reported in a few cases of syndromic autosomal recessive ciliopathies, such as orofaciodigital syndrome type-IX (OFD-IX; OMIM# 258865), characterized by developmental defects of the oral cavity (e.g., cleft palate), facial features, digital abnormalities, and retinal defects[7,8], Bardet-Biedl syndrome (BBS; OMIM PS209900), characterized by RCD, truncal obesity, cognitive impairment, hypogonadism in men, digital and renal abnormalities[9], and Senior-Løken syndrome (SLS; OMIM PS266900), hallmarks of which are nephronophthisis and early-onset severe retinal dystrophy (EOSRD)[10,11].

Ciliopathy cases harboring pathogenic *SCLT1* variants have been described[12–21]. However, in 2016, De Castro Miró and colleagues described two siblings with early-onset RCD in one Argentinian family carrying compound heterozygous variants in *SCLT1*[22], and very recently, a third compound heterozygous non-syndromic IRD patient was reported from a large mutational screen of 1000 affected cases[23]. However, a conclusive association of *SCLT1* mutations with non-syndromic IRD has never been reached due to the small number of non-syndromic cases. In this study, we describe five new families with non-syndromic IRD and one additional proband with a milder syndromic IRD. This further defines the phenotype spectrum for bi-allelic variants in *SCLT1*. We also report eight novel variants in this gene, three of which are likely pathogenic.

Results

Rare *SCLT1* variants associated with non-syndromic IRD

By analyzing data from either targeted next generation sequencing, exome sequencing (ES), or genome sequencing (GS) of a cohort of ~8500 mostly non-syndromic IRD cases, we identified six probands (Family 1_II-3, Family 2_II-4, Family 3_II-1, Family 4_II-1, Family 5_II-1, Family 6_II-1) with rare bi-allelic *SCLT1* variants (V1-10, MAF < 0.00001997) (see Fig. 1A and Table 1). No additional disease-causing variants were present in any of the currently known IRD genes[24] that could explain the clinical phenotype.

Of the ten likely causal variants found in *SCLT1*, four were missense (c.1631A>G p.(Lys544Arg); c.439G>T p.(Ala147Ser); c.671T>G p.(Leu224Arg); c.1706G>A p.(Ser569Asn)), two were single amino acid deletions (c.165_167del p.(Phe55del); c.778_780del p.(Glu260del)), three were non-coding variants c.290+2732A>G, c.778-2A>T, and c.1439+5G>T located in intron 5, 10, and 16, respectively, and one was an exon 3-10 tandem duplication (chr4:128968796_129045332dup).

All variants were novel, except for c.778-2A>T and c.1631A>G p.(Lys544Arg). The c.778-2A>T variant was detected in two siblings with early-onset RCD[22], while the p.(Lys544Arg) was first reported in syndromic

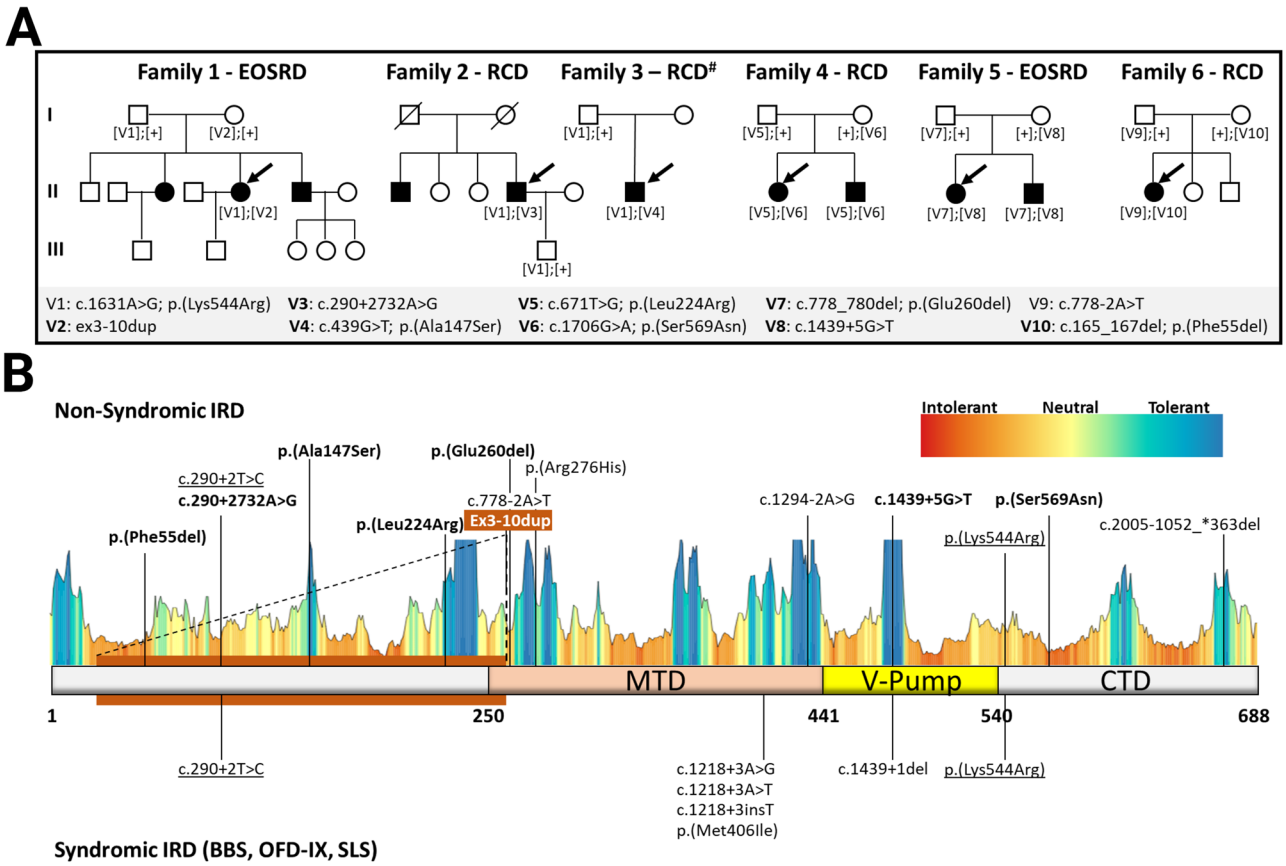

Fig. 1 | Pedigrees of the *SCLT1* families described in this study. A For each family (1-6), the specific IRD phenotype diagnosed is mentioned above each pedigree (EOSRD, early-onset severe retinal dystrophy; RCD, rod-cone dystrophy; RCD#, mildly syndromic RCD phenotype with mild intellectual disability and cleft palate). Affected male and female subjects are represented with black squares or circles, respectively. Probands are indicated by a black arrow. Novel variants (V2-V8, V10) are indicated in bold. All presented variants refer to the *SCLT1* transcript NM_144643.4. Bi-allelic inheritance was confirmed by familial segregation analysis in all families. **B** SCLT1 secondary structure and distribution of known and novel disease variants found in affected individuals. The prediction model of the mutation tolerance landscape of the SCLT1 protein was retrieved from the MetaDome webpage. Protein motifs and catalytic domains are highlighted using different colors, while variants were divided in two groups, depending on whether they were found in syndromic or non-syndromic IRD patients. Known variants were retrieved from the Leiden Open Variation Database (LOVD). Novel variants reported in this study are in bold, while the known variants c.778-2A>T and p.(Lys544Arg), present in both patient groups, are highlighted. OFD-IX orofaciodigital syndrome type-IX, BBS Bardet-Biedl syndrome, SLS Senior-Løken syndrome, MTD myosin taildomain, CTD C-terminal domain. Figure was created using Biorender software.

https://doi.org/10.1038/s41525-026-00566-z

Table 1 | Clinical characteristics and *SCLT1* variants of the IRD patients of our study cohort

Family_ patient	Research_ID	Age at initial visit | sex	Diagnosis	Ethnicity	Non-retinal features	Ocular symptoms	BCVA	*SCLT1* variants	GnomAD v4_ AF | AC	ACMG	Associated phenotype(s)
1_II-3	URDGH_005	43 | F	EOSRD	South Korean	None	Poor vision since age 8–9, nystagmus	Age 43: LP − OD LP + OS	**V1**: c.1631A>G; p.(Lys544Arg)	0.00001997 | 32 (30 EAS, 2 n-FE)	**LP** (PS3; PM2; PM3sup; PP1; PP3)	EOSRD[b]; RCD; SLS + LCA[15] BBS + RCD[18,19]
								V2: ex3-10dup (chr4:128968796_ 129045332dup)[a]; p.?	n.a.	**LP** (PM1; PM2; PM3; PM4)	EOSRD[b]
2_II-4	URDGH_033	57 | M	RCD	South Korean	None	Poor vision since age 55	Age 57: 20/ 25 OU	**V1**: c.1631A>G; p.(Lys544Arg)	0.00001997 | 32 (30 EAS, 2 n-FE)	**LP** (PS3; PM2; PM3sup; PP1; PP3)	EOSRD[b]; RCD; SLS + LCA[15] BBS + RCD[18,19]
								V3: c.290+2732A>G; p.?	n.a.	**VUS** (PS3; PM2)	RCD[b]
3_II-1	KA559	22 | M	RCD[#]	Japanese	ID, cleft palate	Nyctalopia and reduced visual acuity since age 13	Age 22: 20/ 100 OD 20/ 80 OS	**V1**: c.1631A>G; p.(Lys544Arg)	0.00001997 | 32 (30 EAS, 2 n-FE)	**LP** (PS3; PM2; PM3sup; PP1; PP3)	EOSRD[b]; RCD; SLS + LCA[15] BBS + RCD[18,19]
								V4: c.439G>T; p.(Ala147Ser)	0.00001752 | 28 (EAS)	**VUS** (PM2)	RCD[b]
4_II-1	OGI163_447	25 | F	RCD	White	None	Nyctalopia since early childhood, reduced side vision since age 16	Age 30: 20/50 OD 20/60 OS	**V5**: c.671T>G; p.(Leu224Arg)	0.000001885 | 3 (n-FE)	**VUS** (PM2; PP1)	RCD[b]
								V6 c.1706G>A; p.(Ser569Asn)	6.22E-07 | 1 (EAS)	**VUS** (PM2; PP1)	RCD[b]
5_II-1	F4419_07910	8 | F	EOSRD	White	None	Poor vision since infancy (15 months), nystagmus	Age 8: 20/500 OD 20/640 OS Age 12: CF OU	**V7**: c.778_780del; p.(Glu260del)	n.a.	**LP** (PS3; PM1; PM2; PM4; PP1)	EOSRD[b]
								V8: c.1439+5G>T; p.?	6.30E-07 | 1 (n-FE)	**LP** (PS3; PM1; PM2; PP1)	EOSRD[b]
5_II-2	F4419_11487	5 | M	EOSRD	White	None	Poor vision since infancy, nystagmus	Age 7: 20/640 OD 20/ 800 OS	**V7**: c.778_780del; p.(Glu260del)	n.a.	**LP** (PS3; PM1; PM2; PM4; PP1)	EOSRD[b]
								V8: c.1439+5G>T; p.?	6.30E-07 | 1 (n-FE)	**LP** (PS3; PM1; PM2; PP1)	EOSRD[b]
6_II-1	MOL1119-1	52 | F	RCD	White	None	Poor vision since age 14	Age 43: 3/60 OD 3/18 OS Age 50: HM OD 6/60 OS	**V9:** c.778-2A>T; p.?	0.000004392 | 7 (3 AMR, 1 n-FE, 3 remaining individuals)	**P** (PVS1; PM2; PP1)	RCD[22,b]
								V10: c.165_167del; p.(Phe55del)	0.000003400 | 5 (3 AMR, 2 n-FE)	**VUS** (PM2; PM3)	RCD[b]

All presented variants refer to the *SCLT1* transcript NM_144643.4.

AC allele count, *ACMG* American College of Medical Genetics, *AF* allele frequency, *AMR* Admixed Americans, *BBS* Bardet-Biedl syndrome, *CF* counting fingers, *EAS* East Asian, *EOSRD* early-onset severe retinal dystrophy, *F* female, *HM* hand motion, *ID* intellectual disability (mild), *LCA* Leber congenital amaurosis, *LP* (in BCVA column), light perception, *LP* likely pathogenic, *M* male, *n.a.* not available, *n-FE* non-Finnish Europeans, *OD* right eye, *OS* left eye, *OU* both eyes, *RCD* rod-cone dystrophy, *RCD#* mildly syndromic RCD phenotype with mild intellectual disability and cleft palate, *SLS* Senior-Løken syndrome, *VUS* variant of uncertain significance.

[a]Breakpoint coordinates obtained based on GATK-SV pipeline.

[b]This study.

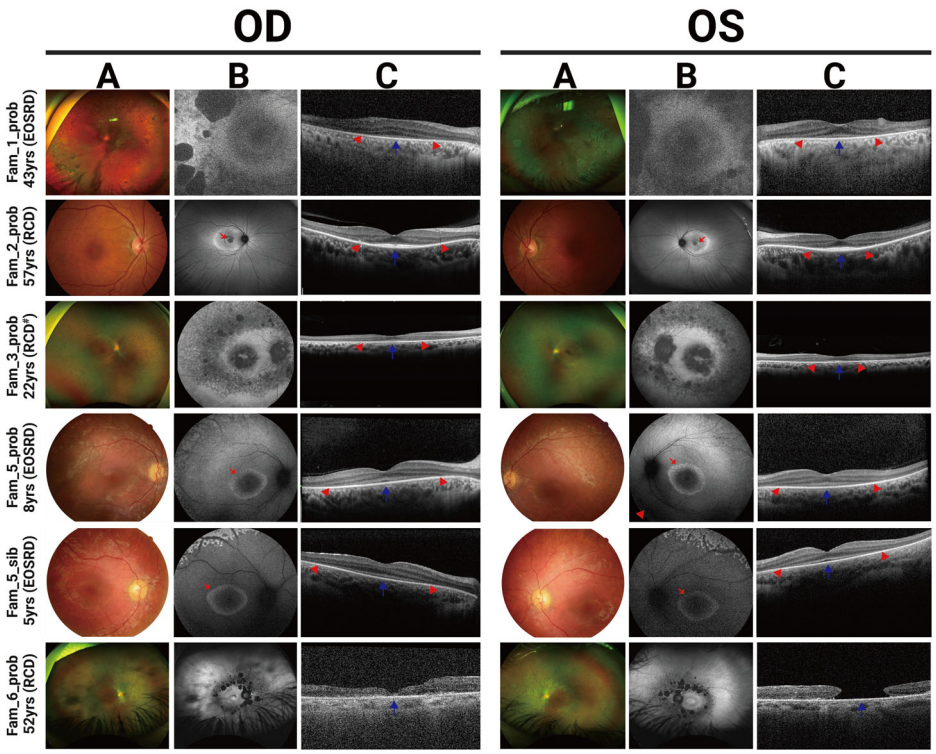

Fig. 2 | Retinal phenotypes of *SCLT1*-IRD patients. Images show fundus photos (**A**), fundus autofluorescence (**B**), and optical coherence tomography (OCT) imaging (**C**) for five probands and the affected sibling of family 5 proband. The age (in years) indicates when the imaging data were obtained, which does not always overlap with the actual age of onset. Imaging showed features consistent with the clinical diagnosis. The specific IRD phenotype of each patient is given in brackets (EOSRD, early-onset severe retinal dystrophy; RCD, rod-cone dystrophy; RCD#, mildly syndromic RCD phenotype with mild intellectual disability and cleft palate). OCT shows disruption of the ellipsoid zone (EZ) with foveal sparing, consistent with rod-cone dystrophy. Red arrowheads indicate the boundaries of the EZ disruption (blue arrow: foveal center). The perifoveal hyperfluorescence ring was noted in 3 patients (red arrow). Patients Fam_1 and Fam_5 were diagnosed with EOSRD based on the presence of nystagmus and early-onset visual impairment. Figure was created using Biorender software.

patients with SLS[15] or BBS[18,19] showing ocular phenotypes of EOSRD or RCD, respectively (see Supplementary Tables 1 and 2). The p.(Lys544Arg) is the second most commonly reported variant in *SCLT1* patients (see Supplementary Tables 1 and 2), and the most recurrent in our cohort: present heterozygously in three East Asian probands (families 1-3, see Fig. 1A). This allele is most likely a founder allele in the East Asian population, given its prevalence in this population (gnomAD v4.1: 30 alleles in total, MAF: 0.0006701), compared to the general population except for the East Asian (2 alleles, MAF: 0.00001997)[25].

Compound heterozygosity was confirmed by familial segregation analysis in all families.

Clinical phenotypes

Six probands (four females and two males) with *SCLT1*-associated disease had a clinical diagnosis of EOSRD or RCD (see Fig. 2, Table 1, Supplementary Fig. 1, and Supplementary Table 3). Five probands manifested the onset of symptoms during infancy (~15 months), childhood, or early teenagerhood (14 years), while family 2 proband reported a late-onset RCD phenotype at age 57 (see Table 1).

Visual acuity was variable across cases. Family 1 proband, diagnosed with EOSRD and presented with light perception when evaluated at age 43, while family 2 and 4 RCD probands showed normal (20/25) or near normal (20/60) visual acuity in each eye at age 57 and 30, respectively.

Visual field data using Goldmann kinetic or Humphrey visual perimetry showed constriction of the visual fields in all probands, except for family 1 proband, for whom testing was not possible due to nystagmus and low vision (see Supplementary Table 3). Family 2 and 6 probands had ring scotoma around the center, while family 3 and 4 probands had constricted visual fields consistent with RCD. Full-field ERGs were available for all patients except for family 1 proband (see Supplementary Table 3). Probands of family 2 and 6 showed varying degrees of scotopic alterations with less severe photopic dysfunction, while probands of family 3, 4, 5, and her brother had severe generalized dysfunction of both scotopic and photopic responses.

Fundus evaluation of family 2 proband was normal, while all other patients showed features that were typical for the retinal degeneration diagnosis (see Fig. 2 and Supplementary Fig. 1). Both siblings of family 5, affected by EOSRD, exhibit a large number of mottled and whitish lesions in the peripheral retina (see Supplementary Fig. 1). Spectralis OCT images were available for five individuals and showed significant alteration of the ellipsoid zone (EZ) bands and outer nuclear layer thinning, with a small island of EZ bands at the foveal center (see Supplementary Table 3). Some of the patients (e.g., proband of family 3 and both siblings of family 5) had better outer retinal structure on OCT than the visual acuity would suggest (see Table 1), indicating an element of structure-function dissociation in this condition. Additional ophthalmic diagnoses included nystagmus in probands of family 1, 5, and her brother, as well as a full-thickness macular hole in both eyes of family 6 proband. Clinical examination of family 3 proband also revealed some degree of intellectual disability and cleft palate, but no other systemic diagnoses of note were present in our probands.

SCLT1 variants leading to splicing defects

Since three variants were located in proximity of canonical splice sites (V1 c.1631A>G p.(Lys544Arg), V7 c.778_780del p.(Glu260del), V8 c.1439+5G>T) and one variant was deep-intronic (V3 c.290+2732A>G), we tested their effects on pre-mRNA splicing with mini-gene constructs in HEK293T cells or by RT-PCR of blood-derived total RNA, when available (see Fig. 3 and Supplementary Fig. 2). Variants were predicted to affect normal splicing according to multiple in silico tools, such as SpliceAI[26], Pangolin[27], and ESEfinder[28] (see Supplementary Table 4).

The c.1631A>G p.(Lys544Arg) variant is located two base pairs (bp) upstream of the canonical donor splice site of exon 17 and is predicted to induce donor loss and activation of an alternative donor splice site located 6-bp upstream, thus resulting in the in-frame deletion of the last 6 nucleotides coding for two amino acid residues (Val543 and Lys544) (see Supplementary Table 4). Transcript analysis using whole blood RNA in families 1 and 2 probands heterozygous for this variant, confirmed a donor loss inducing exon 17 skipping, leading to frameshift (p.Asp480Glufs*11) in most of transcripts (see Fig. 3A), and a 6-bp deletion event in some of them (see Supplementary Fig. 3). These results validated the main molecular defect described by Katagiri and colleagues[15].

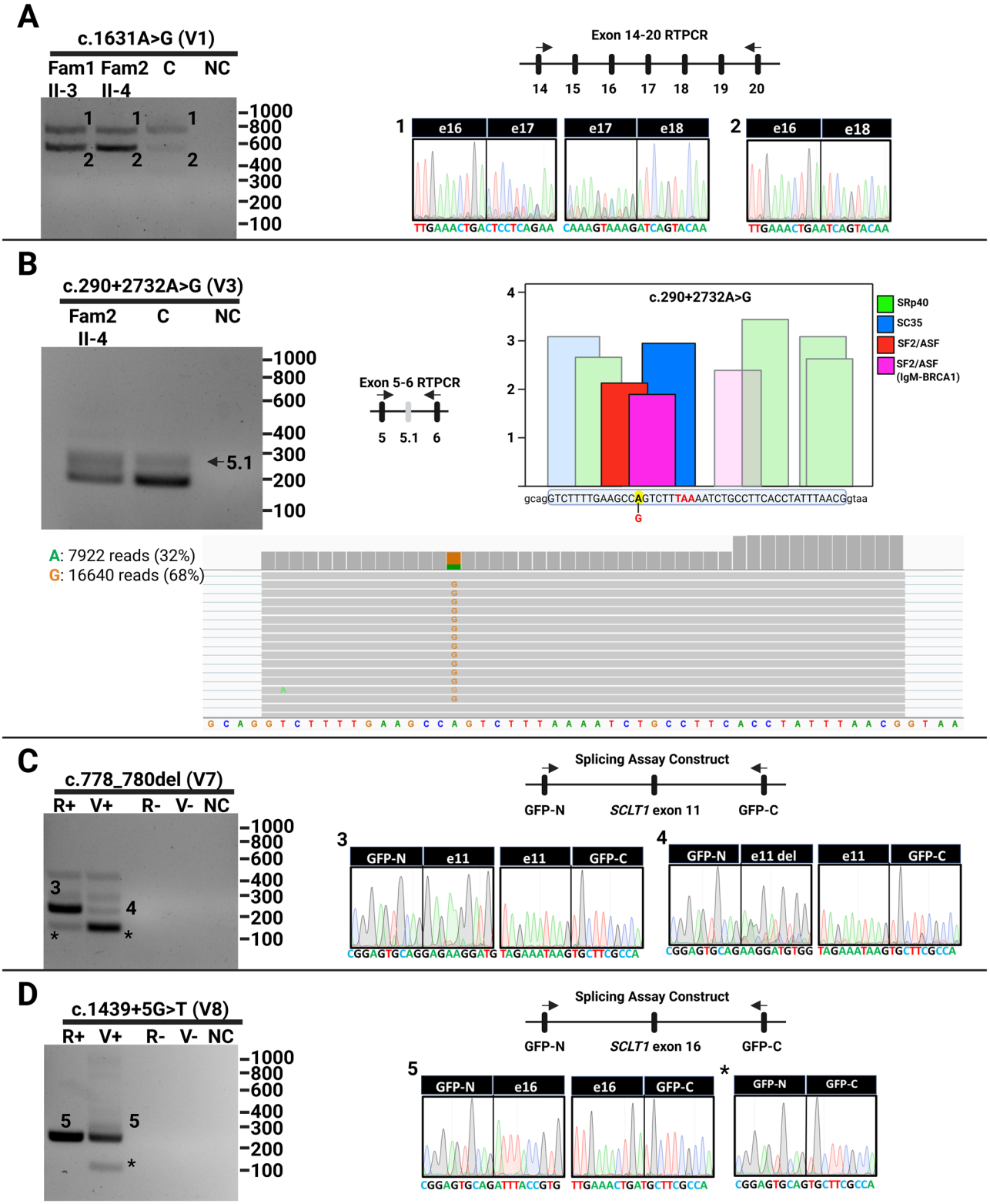

The deep-intronic variant c.290+2732A>G resulted in the partial inclusion of a 45-bp cryptic exon in intron 5, containing a stop codon. Although the SpliceAI predictions were low (simultaneous acceptor and donor gain with scores of 0.16 and 0.15, respectively) (see Supplementary Table 4), the A > G transition was predicted by ESEfinder to enhance the binding of three exonic splicing enhancers (ESEs) located within the cryptic exon (see Fig. 3B). The presence of the cryptic exon 5 was validated by RT-PCR of family 2 proband and control blood-derived RNA. Even though the cryptic exon inclusion was seen in both samples, the NGS quantification of cryptic exon reads, including the reference allele (c.290+2732 A, 32%) compared to the variant allele (c.290+2732 G, 68%), revealed two-fold enrichment in the cryptic exon inclusion due to the c.290+2732A>G variant. Next-generation sequencing of the amplified product also confirmed the cryptic exon size of 45 bp (see Fig. 3B).

Fig. 3 | Functional validation of *SCLT1* splicing variants. A Transcript analysis of variant c.1631A>G p.(Lys544Arg) using primers spanning *SCLT1* exon 14 and 20. RT-PCR revealed exon 17 skipping in probands of families 1 and 2, heterozygotes for the variant, compared to the reference control (C) and negative control (NC). RT-PCR bands were purified and sequenced, confirming the splicing defects. **B** Transcript analysis of variant c.290+2732A>G using primers spanning *SCLT1* exon 5 and 6. RT-PCR revealed cryptic exon 5.1 inclusion skipping in proband II-4 of family 2, heterozygote for the variant. The transcript defect was also detected in the RNA of the healthy control (C) who did not carry the variant, although its intensity was reduced. ESEfinder analysis of the 45-bp cryptic exon activated by the deep-intronic variant c.290+2732A>G compared to the reference sequence. The A > G transition does not occur at the splicing boundaries and leads to the activation of SC35 and SF2/ASF exonic splicing enhancers (ESEs). Next-generation sequencing was used to quantify the percentage of reads showing cryptic exon inclusion, which accounted for 68%. **C** Reference (R) and mutant (V) splicing constructs for variants c.778_780del p.(Glu260del), and c.1439+5G>T (**D**) were designed, transfected in HEK293-T cells and assayed for splicing defects. Transcript analysis by RT-PCR (+ and – refer to RT+ and RT-) using primers spanning the flanking GFP exons unraveled pre-mRNA defects for both *SCLT1* variants. RT-PCR bands were purified and sequenced, confirming the splicing defects. Figure was created using Biorender software.

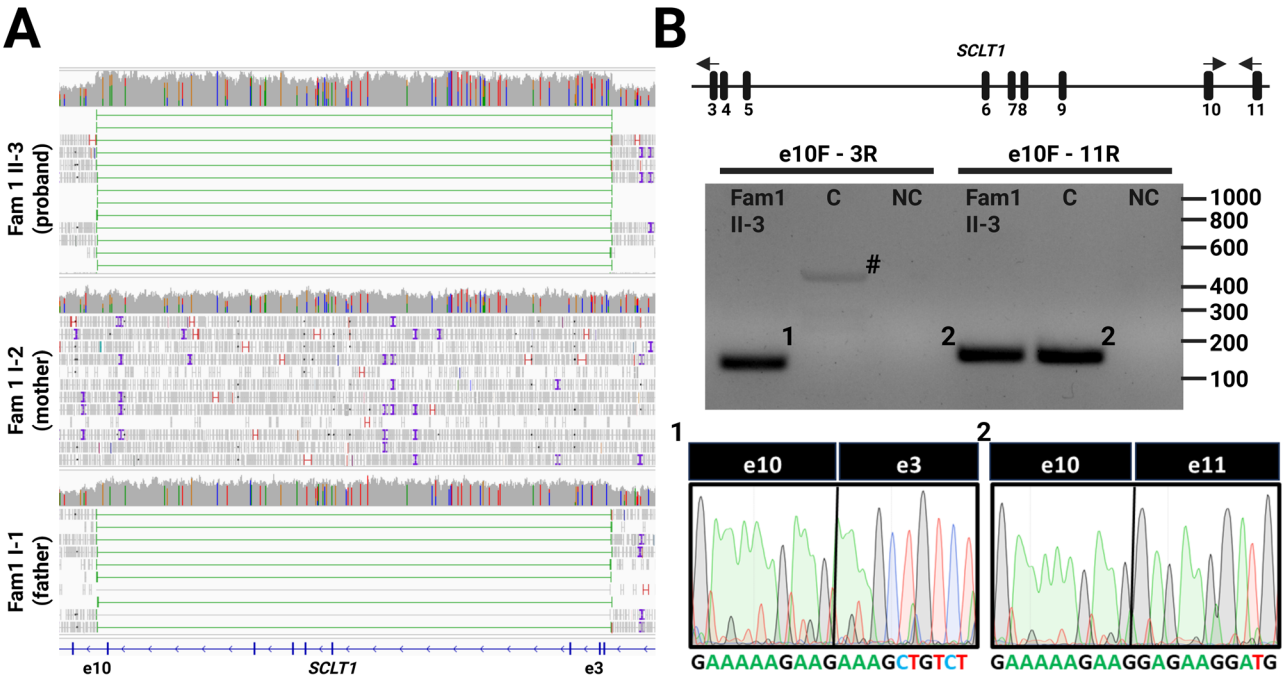

Fig. 4 | Analysis of the SCLT1 exon 3-10 in-frame tandem duplication detected in proband I-3. A IGV tracks showing the segregation of the tandem duplication in Family 1. Indeed, the structural variant is detected in the proband and her father (healthy carrier) but not in her mother. **B** RT-PCR-based validation of the duplication breakpoint in proband II-3 using ad hoc primers spanning exon 3 and exon 10. The resulting ~150-bp amplicon could be detected in the proband, but it is absent when using a control (C) sample and a negative control (NC). A control RT-PCR amplicon encompassing exons 10 and 11 showed no difference between the proband and control samples. Figure was created using Biorender software.

The splicing effect of variants c.778_780del p.(Glu260del) and c.1439+5G>T were assessed via mini-gene-based splicing assay. The first variant removes the first three bp of exon 11, leading to exon 11 skipping, with a smaller fraction of the transcripts still containing the exon but lacking the Glu260 (see Fig. 3C). The c.1439+5G>T variant, located in intron 16, showed an incomplete missplicing effect with partial skipping of exon 16, consistent with the Pangolin prediction (splice loss 0.65). The same donor loss was not predicted by SpliceAI (0.12), which instead predicted a donor gain 80-bp upstream (0.33) of the variant, not confirmed by the splicing assay (see Fig. 3D and Supplementary Table 4).

Due to the partial effect on cryptic exon inclusion, we consider the c.290+2732A>G as a hypomorphic variant, classified as a variant of uncertain significance (VUS) according to the ACMG guidelines, while the other three variants were classified as likely pathogenic (see Table 1). When splicing assay for these variants was performed in WERI-Rb1, a cell line derived from retinoblastoma cells, we obtained similar results (see Supplementary Fig. 4).

Detection of a large structural variant in *SCLT1*

Structural variants (SVs) analysis of the GS data in the proband of family 1 by the GATK-SV pipeline led to the identification of a novel ~76 kb duplication (chr4:128,968,796_129,045,332dup) encompassing the genomic sequence between exon 3 and 10 of *SCLT1* and never reported in gnomAD SVs v4.1 (see Figs. 1 and 4A).

This SV is supported by B-allele frequency, paired-end, read-depth, and split reads on both SV sides (see Fig. 4A). Although the lack of additional patient DNA did not allow us to Sanger validate the breakpoint coordinates provided by the GATK-SV pipeline, we were able to demonstrate the exon 3-10 in-frame duplication by RT-PCR using patient blood-derived RNA (see Fig. 4B). Using primers spanning the predicted duplication boundary, we amplified a 142-bp fragment corresponding to the exon 10 - exon 3 splicing boundary (see Fig. 4B). This fragment was specific to the patient RNA and was not detected using control human RNA. The coding effect of this novel SV consists in the incorporation of 225 amino acids (Lys35 - Lys259) between residue Lys259 and Glu260, which are part of the Myosin Tail Domain (MTD). In the absence of a SCLT1 protein structure model on Protein Data Bank, we used the Alphafold Server3 (https://alphafoldserver.com) to evaluate the structural changes caused by the in-frame exon 3-10 duplication (see Supplementary Fig. 5). Increased intra-protein interactions were predicted following the SCLT1 exon 3-10 duplication. Furthermore, the wild-type elongated linker protein is predicted to become shortened due to the duplication, potentially leading to a loss of function.

Protein modelling and genotype-phenotype correlation analysis

Variants in *SCLT1* have been associated with syndromic forms of retinal degeneration. To investigate whether this phenotypic variability was the consequence of a specific variant localization, we plotted the known 11 *SCLT1* variants reported in the literature and the eight novel variants detected in our probands onto the secondary structure of the human SCLT1, a 688 amino acid protein (UniProtKB ID: Q96NL6) (see Fig. 1B and Supplementary Table 1)[12–23]. A third of the 19 analyzed *SCLT1* variants were missense, while the others were either truncating or non-coding variants. Variants were equally distributed within the secondary structure of the protein, affecting either its disorganized N-terminal region (residues 1-250) and the three functional domains located at the central (MTD) and C-terminal (V-pump and CTD) region (see Fig. 1B). Of note, all variants associated with syndromic phenotypes were splice variants affecting the donor splice site, located either at the terminal of an exon (c.1218G>A p.Met406Ile and c.1631A>G p.Lys544Arg) or at conserved intronic positions +1, +2, and +3, suggesting a severe truncating effect. Among the variants associated with non-syndromic IRDs there were five missense changes and splicing variants with incomplete effect, such as the c.290+2732A>G and the c.1439+5G>T (see Fig. 3). The mutation tolerance at SCLT1 protein residues was analyzed using MetaDome (https://stuart.radboudumc.nl/metadome/)[29], while the impact of specific missense variants on SCLT1 structure and function was predicted by tools like SIFT[30], PolyPhen2[31], CADD Phred[32], and REVEL[33] (see Supplementary Table 5). The five missense variants (p.Ala147Ser, p.Leu224Arg, p.Arg276His, p.Lys544Arg, p.Ser569Arg) present in non-syndromic cases, four of which identified in our patients, were all predicted deleterious by CADD Phred, and by at least one between SIFT or PolyPhen2 prediction programs, but not by Revel (see Supplementary Table 5). Moreover, three of them (p.Ala147Ser, p.Leu224Arg, p.Arg276His), were also located in residues predicted to be tolerant toward mutations (see Fig. 1B). The p.(Lys544Arg), enriched among the East Asian population, was the only variant shared between non-syndromic and syndromic cases. In particular, it was detected heterozygously in two unrelated Japanese families with BBS plus RCD[18] and in a third Japanese family with SLS plus EOSRD[15] (see Fig. 1B and Supplementary Table 1).

Thus, after comparing genotypes of all previously reported and new 24 cases carrying bi-allelic *SCLT1* variants (see Supplementary Table 1), we observed an enrichment of hypomorphic alleles in non-syndromic IRD patients compared to syndromic *SCLT1* patients.

Discussion

In this study, we describe six probands with clinical phenotypes of retinal degeneration (EOSRD or RCD) associated with rare bi-allelic variants in *SCLT1*, a gene first associated with autosomal recessive syndromic ciliopathies OFD-IX, BBS, and SLS. We identified eight novel variants, confirmed splicing defect for four variants, and detected a ~ 76 kb in-frame tandem duplication encompassing exon 3-10 of the gene. Our study thus further supports the association of *SCLT1* variants with presumed non-syndromic IRDs first described by De Castro-Miró and colleagues[22] and expands the number of such cases.

Both the deep-intronic c.290+2732A>G and the tandem duplication are, to our knowledge, the first variants of their class to be described in *SCLT1* (see Supplementary Table 1). However, although for the first one it was possible to experimentally validate its pathogenicity, that was not possible for the structural variant. The in-frame tandem duplication is not predicted to disrupt any known protein domains, yet it is predicted to double the N-terminal region, extending the protein by 30% of its original length and increasing the number of intra-protein interactions. Therefore, misfolding followed by subsequent protein degradation is a likely molecular consequence for this structural variant.

By comparing the variants identified in presumed non-syndromic *vs* syndromic patients and their location on the secondary structure of SCLT1 protein, we did not identify a clear mutation hotspot able to explain the different clinical phenotypes. However, by looking at all the bi-allelic combinations in currently reported syndromic cases, we noted a clear enrichment for bi-allelic null alleles, and hypothesize a model in which at least one hypomorphic allele may alleviate the syndromic phenotype and lead to an isolated retinal degeneration (see Fig. 1B). This phenomenon has been observed in other autosomal recessive ciliopathy genes, for which the specific allelic combination found in patients influences their clinical phenotype[34–36]. However, with only 24 *SCLT1* patients described thus far, we cannot draw final conclusions, and additional cases will be needed to support our observation. Equally, we cannot rule out the presence of genetic modifiers of disease severity[37].

With the exception of the family 2 proband, a notable feature in our study cohort was the early disease onset, with symptoms beginning before the age of 14 and as early as 15 months, in the siblings of family 5. In the latter family, the large number of mottled and whitish lesions in the peripheral retina resembled those described in early fundoscopies of LCA patients harboring bi-allelic variants in *IQCB1* and *CEP290*, other ciliopathy genes[38,39]. The early-onset retinal disease observed in our cases overlaps with the previous ophthalmic diagnoses of *SCLT1* patients.

None of the probands in our cohort presented with syndromic symptoms, except for the family 3 proband, in whom mild intellectual disability and cleft palate were noted. Although these extraocular phenotypes overlap with OFD-IX features, they are milder than reported for this syndrome, and they do not include all of the OFD-IX symptoms[7,8].

The most recurrent allele in our study cohort was the known variant c.1631A>G p.(Lys544Arg), found in two South Korean and one Japanese family (Family 1-3). This variant is currently the second most recurrent *SCLT1* allele in patients (second only to c.290+2T>C, see Supplementary Tables 1 and 2), yet it is undoubtedly the most frequent in the general population based on gnomAD v4.1 data (AF = 0.00001997 *vs* AF = 6.586e-7 of c.290+2T>C). That is likely due to its enrichment among the East Asian population, especially in Japan, where this allele has an allele frequency of 0.1%[40].

Using cDNA from two different probands carrying the c.1631A>G p.(Lys544Arg) variant, we have independently validated the finding by Katagiri and colleagues[15], that the variant leads to a partial exon 17 skipping (see Fig. 3A). Since functional characterization of this variant was performed on blood-derived RNA, we cannot be sure which of the effects is predominant in human photoreceptors: exon skipping or the p.(Lys544Arg) missense. Both events will affect the C-terminal domain, an area that is predicted to poorly tolerate change, and is known (amino acids 541-688) to contain dileucine motifs that may bind clathrin[41] and AP2 complex[42]. Therefore, both the exon 17 deletion and the missense variant are likely to be pathogenic.

Of the eight novel variants reported in our study, only three were likely pathogenic, while three missense (p.Ala147Ser, p.Leu224Arg, p.Ser569Asn), one single amino acid deletion (p.Phe55del), and the deep-intronic variant c.290+2732A>G were classified as VUS. The p.(Leu224Arg) and p.(Ser569Asn) were found in the family 4 proband and her brother, and were proven to be in *trans*. The proband of this family presented with an early-onset disease. The p.(Ser569Asn) is located in the CTD domain and predicted to be in a less mutation-tolerant region, according to MetaDome (see Fig. 1B). Regarding the p.(Ala147Ser) and the c.290+2732A>G, we could hypothesize a milder effect for both alleles, as they were detected in patients with the age of onset of 13 and 55 years, respectively. The p.(Ala147Ser) was predicted to modify a tolerant region and transcript analysis of c.290+2732A>G showed a moderate effect, suggesting that both variants could act as hypomorphic alleles. Both alleles were found in *trans* with the severe variant p.(Lys544Arg), indicating that a likely hypomorphic second allele could induce a milder retinal disease phenotype. Moreover, it is important to mention that under the experimental settings of our mini-gene splicing assay, the strength of the observed splicing effect is approximate and we cannot rule out that the c.290+2732A>G might have a more severe molecular effect when tested in a larger genomic context and in the retina.

In conclusion, our data defines a phenotype spectrum caused by pathogenic variants in *SCLT1* and expands the mutation landscape by

providing novel coding and non-coding variants in this ciliopathy gene. *SCLT1* variants are associated with a range of syndromic ciliopathies, early onset and later onset IRD.

Methods

Ethics statement

The study was approved by the institutional review board of all participating institutions (Institutional Review Board of Gangnam Severance Hospital: 3-2021-0153 for families 1 and 2, NHO Tokyo Medical Center (Reference; R19-030, R 21-108, R22-028) for family 3, Partners HealthCare System for family 4, Committees of Protection of Persons Ile de France V for family 5, and Hadassah Hospital Institutional Review Board for family 6) and adhered to the Declaration of Helsinki. Informed consent was obtained from all individuals on whom genetic testing and further molecular evaluations were performed.

Clinical evaluation

Six probands with autosomal recessive RCD or EOSRD were enrolled in this study. Two of them were ascertained from Gangnam Severance Hospital, while the other four from NHO Tokyo Medical Center, Massachusetts Eye and Ear, the National Reference Centre of Rare Diseases at Quinze-Vingts National Hospital, and Hadassah Medical Center.

Clinical evaluation was performed by experienced ophthalmologists according to previously published protocols and included functional and structural assessments[43–46]. Visual acuity was measured using Snellen and Early Treatment of Diabetic Retinopathy Study (ETDRS) charts. Kinetic perimetry was performed using a Goldmann perimeter or Humphrey perimeter (in family 2 proband only). Full-field electroretinograms (ERG) were performed using Burian-Allen electrodes and a custom ERG system. Retinal structure was assessed with fundus photography (Topcon Medical Systems, New Jersey, USA; Optos, Massachusetts, USA), spectral-domain optical coherence tomography (SD-OCT: Spectralis, Heidelberg Engineering, Germany; Cirrus, Carl Zeiss, Meditec, Germany), and fundus autofluorescence (FAF; Spectralis, Heidelberg Engineering, Germany; Optos, Massachusetts, USA).

Genetic analysis

Blood samples were obtained from probands, and when possible, their parents. DNA was isolated from peripheral blood lymphocytes by standard procedures. GS for probands of families 1 and 2 was performed at Theragen Bio (Seongnam-si, South Korea). GS data was aligned to hg38, and variant calling was performed using DRAGEN-GATK4 best practice. GATK-structural variant (SV) cohort mode using 5 different algorithms was used for structural variant calling[47]. Family 4 proband is part of a historical cohort that underwent clinical evaluation in the Inherited Retinal Disorder Service (at MEE; Boston, MA) in the 1990s and early 2000s. Exome sequencing (ES) for this proband was performed at the Center for Mendelian Genomics at the Broad Institute of the Massachusetts Institute of Technology and Harvard using methodology described previously[48]. ES data were aligned to hg38, and variants were called using the GATK HaplotypeCaller package version 3.5 (https://software.broadinstitute.org/gatk/). Data were displayed and analyzed with an online tool (https://seqr.broadinstitute.org)[49]. All sequencing data were filtered for rare variants (AF < 0.001 in GnomAD v4 database), and likely pathogenic variants in all reported IRD genes[24] were excluded.

Family 5 proband was screened applying a customized NGS panel as reported before[50] updated regularly to include newly IRD-associated genes, while NGS-based testing was performed by commercial diagnostic laboratories (Blueprint Genetics) for the proband in family 3. Family 6 proband was screened by both WES (3billion) and WGS (CNAG, Spain) and analyzed through the Genoox pipeline (https://franklin.genoox.com/), including copy number variation analysis.

To detect possible copy number variations, gCNV software was used as before[51]. Relatedness of the sequenced families was excluded using Peddy[52].

Variant validation and phasing

All presented variants refer to the *SCLT1* transcript NM_144643.4. Variant segregation was performed by Sanger sequencing (see Supplementary Table 6 for sequencing primer) or analysis of NGS reads. Sanger sequencing was performed on ABI 3730xl (Applied Biosystems) using BigDye Terminator v3.1 kits (Life Technologies). Sequence analysis was done using SeqManPro (Lasergene 11, DNAStar, Madison, WI, USA).

Mini-gene splicing assay

A mini-gene splicing assay was performed using a mini-gene split GFP construct[53], in which N and C-terminal parts of the GFP gene were separated by SMN1 introns 7 and 8 (NM_000344). Reference and mutated gene fragments containing 400–500 bp, including and surrounding intron 5, exons 11, 16, or 17 of the *SCLT1* gene, flanked with 30 bp vector homology arms, were synthesized (TWIST Bioscience, USA) and cloned into the mini-gene construct (Gibson Assembly Master Mix, New England Biolabs). After Sanger sequencing verification of all constructs, they were transfected into the HEK293 cells (Lipofectamine 3000, Thermo Fisher Scientific). Forty-eight hours post-transfection, total RNA was extracted from the transfected cells (RNAeasy Mini Kit, Qiagen) and cDNA was generated using random hexamer primers (SuperScript IV Synthesis Kit, Thermo Fisher Scientific). Subsequently, the mini-gene transcripts were amplified from the cDNA using primers specific to the split GFP fragments (F: 5'- CACACTGGT-GACAACATTTACATAC-3'; R: 5'- GAAATCGTGCTGTTTCATGT-GATC-3'). The PCR products were column-purified (DNA Clean & Concentrator-5, Zymo Research) and analyzed by Sanger sequencing.

Protein modelling, prediction of missense variants, and variant classification

The mutation tolerance at *SCLT1* protein residues was analyzed using MetaDome (https://stuart.radboudumc.nl/metadome/)[29], while the impact of specific missense variants on *SCLT1* structure and function, was predicted by using five prediction algorithms: SIFT[30], PolyPhen2[31], CADD Phred[32], REVEL[33], and EVE[54]. Variants were finally classified according to the ACMG guidelines[55]. Protein modelling of SCLT1 was done with Alphafold3 and UCSF Chimera X[56,57].

Data availability

Variants are available through dbGAP (phs001272.v1.p1 and phs002459.v1.p1) and ClinVar (accession numbers SCV007096065-SCV007096073).

Code availability

Software used in this study: Biorender; SeqManPro (Lasergene v11); Seqr (https://seqr.broadinstitute.org/); UCSF Chimera X.

Received: 22 April 2025; Accepted: 18 March 2026;
Published online: 10 April 2026

References

1. Berger, W., Kloeckener-Gruissem, B. & Neidhardt, J. The molecular basis of human retinal and vitreoretinal diseases. *Prog. Retin. Eye Res.* **29**, 335–375 (2010).
2. Georgiou, M. et al. Phenotyping and genotyping inherited retinal diseases: molecular genetics, clinical and imaging features, and therapeutics of macular dystrophies, cone and cone-rod dystrophies, rod-cone dystrophies, Leber congenital amaurosis, and cone dysfunction syndro. *Prog. Retin. Eye Res*. **100**, (2024).
3. Eggenschwiler, J. onathanT. & Anderson, K. V. Cilia and developmental signaling. *Annu. Rev. Cell Dev. Biol.* **23**, 345–373 (2007).
4. Reiter, J. F. & Leroux, M. R. Genes and molecular pathways underpinning ciliopathies. *Nat. Rev. Mol. Cell Biol*. **18** (2017).
5. Liu, C. et al. CAP-1A is a novel linker that binds clathrin and the voltage-gated sodium channel Nav1.8. *Mol. Cell. Neurosci.* **28**, 636–649 (2005).

6. Tanos, B. E. et al. Centriole distal appendages promote membrane docking, leading to cilia initiation. *Genes Dev.* **27**, 163–168 (2013).
7. Gurrieri, F. et al. Possible new type of oral-facial-digital syndrome with retinal abnormalities: OFDS type (VIII). *Am. J. Med. Genet.* **42**, 789–792 (1992).
8. Nevin, N. C., Silvestri, J., Kernohan, D. C. & Hutchinson, W. Oral-facial-digital syndrome with retinal abnormalities: OFDS Type IX. A further case report. *Am. J. Med. Genet.* **51**, 228–231 (1994).
9. Forsythe, E. Beales, P. Bardet-Biedl Syndrome. in (eds. MP, A. & Ardinger HH, Pagon RA, E) 1993–2019 (GeneReviews®., 2003).
10. Hanssen, O., Halvorsen, S. & Jolster, N. J. A. C. L. Hereditary renal dysplasia and blindness. *Acta Paediatr.* **50**, 177–184 (1961).
11. Senior, B., Friedmann, A. I. & Braudo, J. L. Juvenile familial nephropathy with tapetoretinal degeneration. A new oculorenal dystrophy. *Am. J. Ophthalmol.* **52**, 625–633 (1961).
12. Adly, N., Alhashem, A., Ammari, A. & Alkuraya, F. S. Ciliary genes TBC1D32/C6orf170 and SCLT1 are mutated in patients with OFD type IX. *Hum. Mutat.* **35**, 36–40 (2014).
13. Shaheen, R. et al. Characterizing the morbid genome of ciliopathies. *Genome Biol.* **17**, 1–11 (2016).
14. Patel, N. et al. Genetic investigation of 93 families with microphthalmia or posterior microphthalmos. *Clin. Genet.* **93**, 1210–1222 (2018).
15. Katagiri, S. et al. Compound heterozygous splice site variants in the SCLT1 gene highlight an additional candidate locus for Senior-Løken syndrome. *Sci. Rep.* **8**, 1–10 (2018).
16. Maddirevula, S. et al. Autozygome and high throughput confirmation of disease genes candidacy. *Genet. Med.* **21**, 736–742 (2019).
17. Shamseldin, H. E. et al. The morbid genome of ciliopathies: an update. *Genet. Med.* **22**, 1051–1060 (2020).
18. Morisada, N. et al. Bardet-Biedl syndrome in two unrelated patients with identical compound heterozygous SCLT1 mutations. *CEN Case Rep.* **9**, 260–265 (2020).
19. Sakakibara, N. et al. Comprehensive genetic analysis using next-generation sequencing for the diagnosis of nephronophthisis-related ciliopathies in the Japanese population. *J. Hum. Genet.* **67**, 427–440 (2022).
20. Gillesse, E. et al. Genome sequencing identifies biallelic variants in SCLT1 in a patient with syndromic nephronophthisis: Reflections on the SCLT1-related ciliopathy spectrum. *Am. J. Med. Genet. Part A* 1–7 https://doi.org/10.1002/ajmg.a.63789 (2024).
21. Grudzinska Pechhacker, M. K. et al. Reduced cone photoreceptor function and subtle systemic manifestations in two siblings with loss of SCLT1. *Ophthalmic Genet.* **45**, 95–102 (2024).
22. De Castro-Miró, M. et al. Novel candidate genes and a wide spectrum of structural and point mutations responsible for inherited retinal dystrophies revealed by exome sequencing. *PLoS One* **11**, 1–19 (2016).
23. Weisschuh, N. et al. Diagnostic genome sequencing improves diagnostic yield: a prospective single-centre study in 1000 patients with inherited eye diseases. *J. Med. Genet*. 1–10 https://doi.org/10.1136/jmg-2023-109470 (2023).
24. Daiger S. P., Sullivan L. S., Bowne S. J., R. B. RetNet. Retinal Information Network. https://sph.uth.edu/retnet/ (1996).
25. Genome Aggregation Database (GnomAD). https://gnomad.broadinstitute.org.
26. Jaganathan, K. et al. Predicting splicing from primary sequence with deep learning. *Cell* **176**, 535–548.e24 (2019).
27. Zeng, T. & Li, Y. I. Predicting RNA splicing from DNA sequence using Pangolin. *Genome Biol.* **23**, 1–18 (2022).
28. Cartegni, L., Wang, J., Zhu, Z., Zhang, M. Q. & Krainer, A. R. ESEfinder: a web resource to identify exonic splicing enhancers. *Nucleic Acids Res.* **31**, 3568–3571 (2003).
29. Wiel, L. et al. MetaDome: pathogenicity analysis of genetic variants through aggregation of homologous human protein domains. *Hum. Mutat.* **40**, 1030–1038 (2019).
30. Kumar, P., Henikoff, S. & Ng, P. C. Predicting the effects of coding non-synonymous variants on protein function using the SIFT algorithm. *Nat. Protoc.* **4**, 1073–1081 (2009).
31. Adzhubei, I., Jordan, D. M. & Sunyaev, S. R. Predicting functional effect of human missense mutations using PolyPhen-2. *Curr. Protoc. Hum. Genet*. https://doi.org/10.1002/0471142905.hg0720s76 (2013).
32. Rentzsch, P., Witten, D., Cooper, G. M., Shendure, J. & Kircher, M. CADD: predicting the deleteriousness of variants throughout the human genome. *Nucleic Acids Res.* **47**, D886–D894 (2019).
33. Ioannidis, N. M. et al. REVEL: an ensemble method for predicting the pathogenicity of rare missense variants. *Am. J. Hum. Genet.* **99**, 877–885 (2016).
34. Nguyen, T. M. T. et al. Missense mutations in the WD40 domain of AHI1 cause non-syndromic retinitis pigmentosa. *J. Med. Genet.* **54**, 624–632 (2017).
35. Sangermano, R. et al. Broadening INPP5E phenotypic spectrum: detection of rare variants in syndromic and non-syndromic IRD. *npj Genomic Med*. **6**, (2021).
36. Coppieters, F., Lefever, S., Leroy, B. P. & De Baere, E. CEP290, a gene with many faces: Mutation overview and presentation of CEP290base. *Hum. Mutat.* **31**, 1097–1108 (2010).
37. Kousi, M. & Katsanis, N. Genetic modifiers and oligogenic inheritance. *Cold Spring Harb. Perspect. Med.* **5**, a017145 (2015).
38. Estrada-cuzcano, A. et al. IQCB1 Mutations in Patients with Leber Congenital Amaurosis. 834–839 https://doi.org/10.1167/iovs.10-5221 (2010).
39. Aleman, T. S. et al. Fleck-like lesions in CEP290-associated Leber congenital amaurosis: a case series. *Ophthalmic Genet* **43**, 824–833 (2022).
40. Mitsuhashi, N. et al. TogoVar: a comprehensive Japanese genetic variation database.1–9 (2022).
41. Angelica, E. C. D. Clathrin-binding proteins: Got a motif? Join the network! **11**, 315–318 (2001).
42. Traub, L. M. Sorting it out: AP-2 and alternate clathrin adaptors in endocytic cargo selection. 203–208 https://doi.org/10.1083/jcb.200309175 (1995).
43. Scott, H. A. et al. Expanding the phenotypic spectrum in RDH12-associated retinal disease. *Cold Spring Harb. Mol. Case Stud.* **6**, a004754 (2020).
44. Moye, A. R. et al. Mutations in ARL2BP, a protein required for ciliary microtubule structure, cause syndromic male infertility in humans and mice. *PLoS Genet.* **15**, e1008315 (2019).
45. Haer-Wigman, L. et al. Non-syndromic retinitis pigmentosa due to mutations in the mucopolysaccharidosis type IIIC gene, heparan-alpha-glucosaminide N-acetyltransferase (HGSNAT). *Hum. Mol. Genet.* **24**, 3742–3751 (2015).
46. Men, C. J. et al. The importance of genetic testing as demonstrated by two cases of CACNA1F-associated retinal generation misdiagnosed as LCA. *Mol. Vis.* **23**, 695–706 (2017).
47. Collins, R. L. et al. A structural variation reference for medical and population genetics. *Nature* **581**, (2020).
48. Zampaglione, E. et al. The importance of automation in genetic diagnosis: Lessons from analyzing an inherited retinal degeneration cohort with the Mendelian Analysis Toolkit (MATK). *Genet. Med.* **24**, 332–343 (2022).
49. Pais, L. S. et al. seqr: A web-based analysis and collaboration tool for rare disease genomics. *Hum. Mutat.* **43**, 698–707 (2022).
50. Audo, I. et al. Development and application of a next-generation-sequencing (NGS) approach to detect known and novel gene defects underlying retinal diseases. *Orphanet J. Rare Dis.* **7**, 1–17 (2012).
51. Zampaglione, E. et al. Copy-number variation contributes 9% of pathogenicity in the inherited retinal degenerations. *Genet. Med.* **22**, 1079–1087 (2020).

52. Pedersen, B. S. & Quinlan, A. R. Who's Who? Detecting and resolving sample anomalies in human DNA sequencing studies with Peddy. *Am. J. Hum. Genet.* **100**, 406–413 (2017).
53. Scott, A. H. et al. A high throughput splicing assay to investigate the effect of variants of unknown significance on exon inclusion. *medRxiv* (2022).
54. Frazer, J. et al. Disease variant prediction with deep generative models of evolutionary data. *Nature* **599**, 91–95 (2021).
55. Richards, S. et al. Standards and guidelines for the interpretation of sequence variants: a joint consensus recommendation of the American College of Medical Genetics and Genomics and the Association for Molecular Pathology. *Genet Med* **17**, 405–424 (2015).
56. Abramson, J. et al. Accurate structure prediction of biomolecular interactions with. *AlphaFold* **3**, 630 (2024).
57. Pettersen, E. F. et al. UCSF ChimeraX: Structure visualization for researchers, educators, and developers. **8**, 70–82 (2021).

Acknowledgements

This work was supported by grants from the National Eye Institute [R01EY035717 (KMB), and P30EY014104 (MEEI core support)], the Foundation Fighting Blindness (EGI-GE-1218-0753-UCSD, KMB), Iraty Award 2023 (KMB), Lions Foundation (KMB), Research to Prevent Blindness Unrestricted Grant (KMB), the Curing Kids Foundation (KMB), and the Horizon Europe Project BETTER (EB and DS). Exome sequencing and analysis were provided by the Broad Institute of MIT and Harvard Center for Mendelian Genomics (Broad CMG) and were funded by the National Human Genome Research Institute, the National Eye Institute, and the National Heart, Lung and Blood Institute grant UM1HG008900 and in part by National Human Genome Research Institute grant R01 HG009141. The authors would like to thank the patients and their family members for their participation in this study and the Ocular Genomics Institute Genomics Core members for their experimental assistance. The authors would like to thank the Exome Aggregation Consortium, the Genome Aggregation Database (gnomAD) and the groups that provided exome variant data for comparison. A full list of contributing groups can be found at http://exac.broadinstitute.org/about and http://gnomad.broadinstitute.org/about. We thank Prof. Dr. Fowzan S. Alkuraya and Lama AlAbdi, PhD, from the Department of Translational Genomics, Center for Genomic Medicine, King Faisal Specialist Hospital and Research Center, Riyadh, Saudi Arabia; Prof. Dr. Naoya Morisada from the Department of Pediatrics, Kobe University Graduate School of Medicine, Kobe, Japan; Dr. Lev Prasov from the Department of Ophthalmology and Visual Sciences, Kellogg Eye Center, University of Michigan, Ann Arbor, Michigan; Prof. Dr. Katarina Stingl and Dr. Susanne Kohl from the University Eye Hospital and the Institute for Ophthalmic Research, Center for Ophthalmology, University of Tübingen, Tübingen, Germany, for their help with the clinical interpretation of some *SCLT1* variants. DNA samples from the French center originate from NeuroSensCol DNA bank (PI: JA Sahel, coPI I Audo, partner with Centre Hospitalier National d'Ophtalmologie des Quinze-Vingts, INSERM and CNRS). Funding from this group came from LABEX LIFESENSES (ANR-10-LABX-65) supported by French state funds managed by the Agence Nationale de la Recherche within the Investissements d'Avenir program (ANR-11-IDEX-0004-0) and IHU FOReSIGHT (ANR-18-IAHU-0001), and from the National Reference Centers for Rare Diseases Program. Funding from the South Korea group came from the Korea Disease Control and Prevention Agency (grant No. 2018-ER6902-02) and the National Research Foundation of Korea grant funded by the Korean government (MIST) (grant No. 2020R1C1C1007965).

Author contributions

R.S. performed most of the experiments, data analysis, and led the manuscript writing. K.F., E.M.P., S.K., E.B., C.Z., and I.A. analyzed clinical data and reviewed the manuscript. S.H.B., J.N., J.V., C.C., S.D.T., and D.S. performed part of the genetic analysis. K.M.B. and J.H. guided the experimental design, aided in variant analysis, and contributed to writing the manuscript.

Competing interests

The authors declare no competing interests.

Additional information

Supplementary information The online version contains supplementary material available at https://doi.org/10.1038/s41525-026-00566-z.

Correspondence and requests for materials should be addressed to Kinga M. Bujakowska or Jinu Han.